Timescales of excited state relaxation in α-$RuCl_3$ observed by time-resolved two-photon photoemission spectroscopy

Dan Nevola,[1,3,5] Alexander Bataller,[1,4] Ankit Kumar,[1] Samanvitha Sridhar,[1,5] Jordan Frick,[1,5] Shaun O'Donnell,[2] Harald Ade,[1,5] Paul A. Maggard,[2] Alexander F. Kemper,[1] Kenan Gundogdu,[1,5] and Daniel B. Dougherty[1,5,*]

[1]*Department of Physics, North Carolina State University, Raleigh, North Carolina 27695, USA*
[2]*Department of Chemistry, North Carolina State University, Raleigh, North Carolina 27695, USA*
[3]*Department of Physics and Material Science, Brookhaven National Laboratory, Upton, New York 11973, USA*
[4]*Department of Nuclear Engineering, North Carolina State University, Raleigh, North Carolina 27695, USA*
[5]*Organic and Carbon Electronics Laboratory, North Carolina State University, Raleigh, North Carolina 27695, USA*

(Received 10 February 2021; revised 28 April 2021; accepted 10 May 2021; published 1 June 2021)

The nonequilibrium properties of strongly correlated materials present a target in the search for new phases of matter. It is important to observe the types of excitations that exist in these materials and their associated relaxation dynamics. We have studied the photoexcitations in a spin-orbit assisted Mott insulator α-$RuCl_3$ using time-resolved two-photon photoemission spectroscopy and transient reflection spectroscopy. We find that photoexcited carriers (doublons) in the upper Hubbard band rapidly relax to Mott-Hubbard excitons on a timescale of less than 200 fs. Subsequently, further relaxation of these lower-energy quasiparticles occurs with an energy-dependent time constant of that ranges from 370 to 600 fs due to exciton cooling. The population of Mott-Hubbard excitons persists for timescales up to several microseconds.

DOI: 10.1103/PhysRevB.103.245105

I. INTRODUCTION

The spin-orbit assisted Mott insulator α-$RuCl_3$ has been intensely investigated as a potential quantum spin liquid [1–3]. In the course of these investigations, it has become clear that the many-body physics in this material that suggests quantum spin liquid behavior is not fully understood. For example, the optical absorption spectrum of α-$RuCl_3$ shows a sharp, rising edge that is reminiscent of a Mott-Hubbard exciton (MHE) [4]. This is a bound state between a doubly occupied and an unoccupied site [5]. Understanding the creation and relaxation of Mott-Hubbard excitons is crucial in the search for new phases of driven correlated matter [6–8] and for potential optical applications [9,10].

The electronic structure of α-$RuCl_3$ is often described as a spin-orbit assisted Mott insulator because, while it is predicted to be a metal in the absence of electronic Coulomb repulsions, adding either of these alone does *not* result in an insulator [11]. Instead, both electron-electron repulsions and spin-orbit interactions work in concert to create an energy gap. From one perspective, the electrons in the t_{2g} orbital set of Ru^{3+} are first split by spin orbit into angular momentum subbands with $j_{\text{eff}} = 1/2$ and $j_{\text{eff}} = 3/2$. Then the $j_{\text{eff}} = 1/2$ band is split [2] by on-site electron-electron interactions parametrized by the Hubbard *U*. The result is the lower Hubbard band (LHB) and the upper Hubbard band (UHB) that typify the Mott insulating state. In the Mott insulator, charged quasiparticles are described as negative doublons (doubly occupied sites) and positive holons (unoccupied sites). These quasiparticles can form MHEs when their Coulomb attractions result in a bound state analogous to excitons in uncorrelated semiconductors.

Detailed theoretical discussion of MHEs in one dimension can be found in work by Essler *et al.* [5], who noted that consideration of an extended Hubbard model with near-neighbor Coulomb interactions, in addition to the on-site Hubbard U, is essential to predicting their binding energy. This can be substantially larger than the binding of energy of excitons in traditional band semiconductors. MHEs in higher dimensions still show these basic properties and they have been predicted [12] to arise from complex, many-body spin and charge correlations. These are also significant factors in the search for new transient magnetic phases of matter [6,8]. Importantly for the work we present here, Al-Hassanieh *et al.* have predicted that MHEs should exhibit long lifetimes due to inefficient coupling to low-energy excitations [13].

The existence of bound doublon-holon optical excitations has been demonstrated experimentally in several oxide materials such as $YTiO_3$ [14], Sr_2CuO_3 [15], and Sr_2IrO_4 [16]. In most cases, direct inspection of the steady-state optical absorption spectrum shows an asymmetric peak that can be assigned as excitonic, especially when observed at low temperatures. In addition, more exotic experimental tools such inelastic x-ray scattering [17,18] and time-resolved three-pulse laser spectroscopy [19] have shown that MHEs in the iridates are influenced by low-energy magnetic excitations but maintain distinct quasiparticle identity. In $LaVO_3$, the relaxation of MHEs has been reported to slow down substantially at low temperatures due to strong coupling with spin and orbital degrees of freedom [20].

The relaxation dynamics of MHEs in correlated materials will be decisive for using external driving to create new

*dbdoughe@ncsu.edu

quantum phases, but is also needed to quantify the strength and nature of complex electronic interactions. For example, there are theoretical predictions that the thermalization timescales for doublons in Mott insulators are exponentially small in the on-site Coulomb repulsion U [21,22]. Such scaling has been observed in cold atoms experiments that explicitly simulate the required Hubbard Hamiltonian [22]. In the case of α-$RuCl_3$, with a large U of about 4.35 eV [23], exponential scaling could result in very long-lived excited doublons. However, if MHE formation provides a route for doublon decay, then the dynamics of initial excitations could be much faster. In this case, the focus of a search for long-lived excitations is transferred from the initial "free" carriers to the excitons themselves. This is the scenario for which we provide experimental evidence in the present work.

Recently, Bittner *et al.* have shown that the tuning of nearest-neighbor Coulomb interaction strength in an extended Hubbard model can lead to enhanced excitonic correlations within the Mott gap. As nonlocal Coulomb interactions increase, the photoinduced excitonic states become very long lived [24]. Therefore, nonlocal interactions could play a significant role in the mechanisms underlying long-lived excitons in Mott insulators. In addition, electron-phonon coupling effects on bound MHEs can be strong enough to lead to long-lived polaronic states as shown in theoretical studies of the Hubbard-Holstein model [25]. Evidently, there are numerous opportunities for realizing long-lived excited states in strongly correlated materials.

In this paper, we quantify several timescales associated with both short and long-lived photoexcited states in α-$RuCl_3$. We connect the ultrafast initial decay of excited doublons in α-$RuCl_3$ to Mott-Hubbard exciton formation using a combination of time-resolved two-photon photoemission (2PPE) and transient reflection measurements. MHE formation occurs from an initial free-carrier population that decays in less than 200 fs and MHEs relax further in ∼370 fs. After this initial relaxation, excitons persist with a *very* long population lifetime of order 500 ps, in qualitative agreement with theoretical predictions [13,24].

II. EXPERIMENTAL METHODS

Crystals of α-$RuCl_3$ were grown using the vacuum sublimation method described previously [26] and confirmed to be dominantly the α-$RuCl_3$ structure by powder x-ray diffraction. The crystals were cleaved with carbon tape in vacuum and photoemission experiments were performed under ultrahigh vacuum ($<2 \times 10^{-10}$ Torr) using a commercial hemispherical analyzer (Specs Phoibos 150) equipped with a 2D charge-coupled device detector. Crystal surface quality was confirmed by low-energy electron diffraction and He I (21.2 eV) angle-resolved photoemission spectroscopy (ARPES). Photoemission energy scales are all referenced to the Fermi energy of a Au(111) crystal.

The pump and probe laser pulses for the 2PPE measurements were obtained using the output of a regenerative amplifier (Coherent, RegA) operating at 800 nm and 250 kHz, which was seeded with 120-fs pulses at 76 MHz from a Ti:sapphire oscillator (Coherent Mira). The 200-fs pulses from the amplifier were split into two beams. The first beam (pump) was sent to an optical parametric amplifier, which provided tunable photon energies from 1.9–2.5 eV. The second beam was sent to a fourth harmonic generation setup (Mini Optics) to generate 6.2-eV pulses (probe). An optical delay line was used to control the time delay between pump and probe pulses for time-resolved 2PPE measurements. The system's energy resolution was 37 meV (full width at half maximum), which was obtained by fitting a step function convolved with a Gaussian distribution to the secondary electron edge. The temporal resolution was ∼400 fs, which we define as the full width of the cross correlation between the pump and probe pulses. Possible effects of space-charge distortion of 2PPE spectra were quantitatively assessed using known scaling laws [27,28] with laser fluence and these control experiments are described in the Supplemental Material as Fig. S1 [29] .All fluence values reported here represent the incident light on the sample.

Transient reflection spectroscopy (TRS) was performed using the same laser system as the 2PPE measurements. The TRS pump energy was set to 3.1 eV using second-harmonic generation from 800-nm pulses, and the probe energies ranged from 0.8–1.6 eV using a nonlinear down-conversion (i.e., white light generation) by focusing 800-nm pulses into a piece of flint glass. The $RuCl_3$ sample was mounted in ambient air. Pump-probe beams were focused onto samples using a microscope objective, which also ensured beam overlap. Transient reflectivity was detected using a monochromator-Ge detector with 1 nm of spectral resolution.

III. RESULTS AND DISCUSSION

A. 2PPE observation of hot carriers in the upper Hubbard band of α-$RuCl_3$

First, we characterize the band structure of α-$RuCl_3$. Figure 1(a) shows the background-subtracted band structure above the Fermi level measured by 2PPE using a 2.5-eV pump pulse at zero delay time. We identify a nondispersive feature ∼1.2 eV above the Fermi level as the UHB, which is in agreement with previous inverse photoelectron spectroscopy results [23]. Figure 1(b) shows the occupied band structure using traditional 21.2-eV photoexcitation and is also in agreement with previous results [23,30]. The band centered at −1.5 eV is the lower Hubbard band that predominantly arises from the occupied $j_{\text{eff}} = 1/2$ d orbitals of Ru^{3+} as expected from first-principles calculations [2].

Figure 2(a) shows the evolution of normalized 2PPE spectra measured at zero pump-probe delay for different pump photon energies (1.9–2.5 eV). For a pump energy of 1.9 eV, the feature associated with the UHB is undetectable. Above this energy, intensity develops monotonically due to pump-induced population of the UHB.

In order to isolate the UHB, a best-fit Tougaard background approach [31] is applied to the data. Figure 2(b) shows a representative spectrum obtained with a 2.5-eV pump (solid blue line) and its associated background (black dashed line). Figure 2(c) shows the results of applying the background subtraction to the curves in Fig. 2(a). The very weak dependence of the peak position on the pump-photon energy proves that this feature is a true intermediate state as opposed to

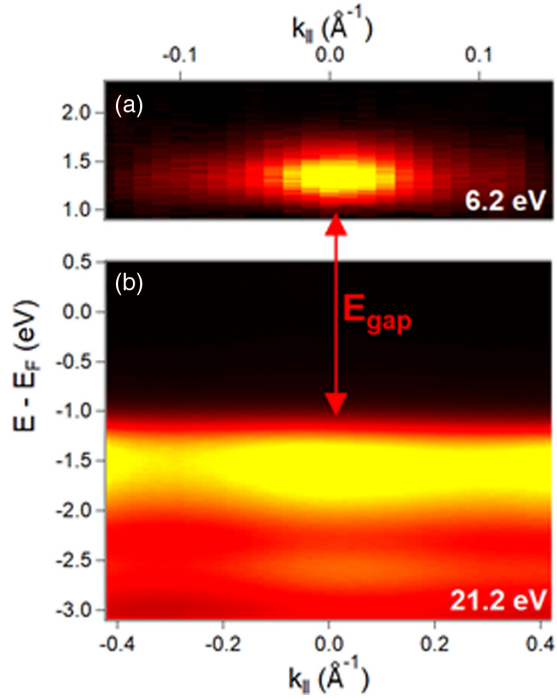

FIG. 1. (a) Background-subtracted 2PPE band map of the UHB region measured with a pump energy of 2.5 eV and a probe of 6.2 eV. (b) 1PPE spectrum measured with 21.2-eV radiation. The energy gap is labeled as the approximate difference between the band edges.

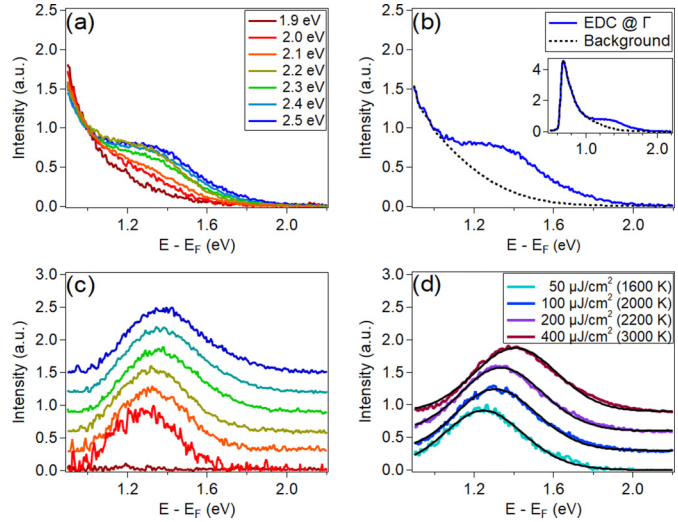

FIG. 2. (a) 2PPE spectra at different pump-photon energies showing the population of the UHB. (b) 2PPE energy distribution curve (EDC) at the zone center for a 2.5-eV pump energy showing the secondary background. Inset: the full energy spectrum showing the secondary electron cutoff. (c) Background-subtracted 2PPE spectra in the region of the UHB for the photon energies in (a). (d) Background-subtracted 2PPE spectra for different pump fluences at 2.5 eV. Colored lines are the data and the black lines are fits to the thermal line shape with hot electron temperatures indicated in the legend.

an occupied initial state since if the latter were the case, the peak position would shift with precisely the change in photon energy. Moreover, the photon energy dependence supports the assignment of the feature at ∼1.2 eV as arising from carriers in the UHB by direct comparison with optical absorption assignments which show a free-carrier feature in this energy range [4]. In particular, the lack of a distinct feature in the 1.1–1.6-eV range when exciting with 1.9-eV pump-photon energy establishes that the feature appearing at higher pump energies is the UHB.

Figure 2(d) shows the results of applying the background subtraction to 2.5-eV pump data at several different pump fluences. It is seen that the peak position in the UHB shifts slightly with pump fluence, similar to what was observed by tuning the pump energy. One possible reason for such a shift is the space-charge distortion when a spatially confined pulse of electrons is photoemitted from the sample. However, the expected dependence of peak shift on pump fluence does not agree with our observations. Space-charge effects typically show a peak shift (and peak width) scaling with number of electrons per pulse as a power law [27,28] with exponent between 0.5 and 1.0 even for pulses photoemitted from insulators [32]. We observe a power-law exponent of 0.1 or lower for the change in peak position and width, so an alternate explanation for the peak shift is more likely.

The observed small size of the peak shift effect can be quantitatively understood as the result of a hot doublon population in the UHB whose precise nonequilibrium temperature depends on excitation density due to the pump pulse. This is the standard approach for characterizing photoexcited states that has been applied to metallic [33–35] and semiconducting materials [36,37]. It identifies a transient difference in temperature between the photoexcited carriers and the other degrees of freedom of the solid, such as phonons, and is often addressed within the two temperature model [38]. Over time, energy exchange between these degrees of freedom brings the solid back to global equilibrium at a single, well-defined temperature.

The black curves in Fig. 2(d) show the result of fitting a thermal line shape for the intensity I of the 2PPE spectrum given by $I(E, T_{\text{eff}}) = I_0 A(E) f(E, T_{\text{eff}})$ [39]. Here, I_0 is the matrix element describing photon absorption and photoionization cross sections, $A(E)$ is the density of states (DOS), and $f(E, T_{\text{eff}})$ is the Fermi-Dirac occupation function corresponding to a "hot" effective temperature T_{eff} that is much higher than the lattice temperature. The solid lines in Fig. 2(d) show fits to this functional form, assuming a Gaussian density of states A with a peak at 1.55 eV that includes the effect of instrument response in its width. The hot electron temperature increases with pump fluence from 1590 to 2950 K [Fig. 2(d)], which is expected when more total excitation density is delivered to the excited population. Such temperature values are similar to those extracted at similar fluences in other quasi-2D materials [40,41]. Thus, the peak-shape changes in Fig. 2(b) arise due to the fluence-controlled thermalization of electrons to very hot effective temperatures on timescales less than 200 fs (see the next section). Note also that the peak-shape changes for different photon energies shown in Fig. 2(c) arise from the same basic hot carrier effect, although in this case the higher excitation density at higher photon energies comes

from the enhanced absorption coefficient known from optical spectroscopy [11].

To further validate the thermalized interpretation of these data, we directly compare the results from Fig. 2 with thermal equilibrium calculations using dynamical mean-field theory (DMFT). The goal of this comparison is not to directly simulate the 2PPE experiment, which would require a more involved nonequilibrium analysis [39]. Instead, we compare the results of an equilibrium calculation at high temperature with the experimental data to support the assertion that the observed population is thermalized.

The single-site impurity problem was solved by the second-order weak-coupling perturbation expansion [6,42]. The parameters of the Hubbard model were chosen to match the experimental width of the UHB and the charge gap. Figure 3 shows the DOS [Fig. 3(a)] and thermal occupation [Fig. 3(b)] *in equilibrium* for the UHB of the strongly interacting Hubbard model. The occupation in Fig. 3(b) shows the same qualitative trends with temperature that the data in Fig. 2(b) show with fluence. However, the DMFT DOS is very different than the experimental DOS so a direct comparison is not possible. Given this limitation, we divided the occupation by the DOS for both theory and experiment, which yields a Fermi function in thermalized circumstances. Figure 3(c) shows the results of this procedure applied to both experiments and simulation when the theoretical and experimental temperatures are similar. The quantitative comparison between the Fermi function in experiment and theory demonstrates the thermalized character of the experiment.

Thermalization leading to the effective Fermi occupation statistics seen in Figs. 2 and 3 requires very rapid exchanges of energy on timescales significantly shorter than the pump-probe cross correlation. This certainly involves intra-Hubbard-band exchange of energy between doublons. Such a process was previously predicted using quantum Boltzmann equation calculations [43] and our experiments provide direct observational evidence that it occurs in real Mott insulators. In addition to this process, α-$RuCl_3$ has several phonon modes at energies in the range of 15 to 80 meV that could provide another mechanism for rapid energy transfers [44]. Very fast phonon-mediated thermalization has been predicted in Mott systems [45]. We note that ultrafast phonon-mediated thermalization of hot electrons in TiO_2 quantum wells has recently been observed [46] and such processes could plausibly contribute to thermalization in our experiments. It would be challenging to experimentally disentangle the relative roles of electron-electron and electron-phonon interaction on ultrafast thermalization in this system without significantly improved time resolution.

Ultrafast thermalization of photoexcited carriers is a common expectation in solids [33,37]. However, it is important that our observations extend this phenomenology to strongly correlated systems and show that the same types of rapid intraband energy exchanges can be operative as known in simple band semiconductors. It is of great interest to control thermalization rates in correlated materials and perhaps access regimes where thermalization can be avoided for long times to preserve and manipulate quantum information. Recent

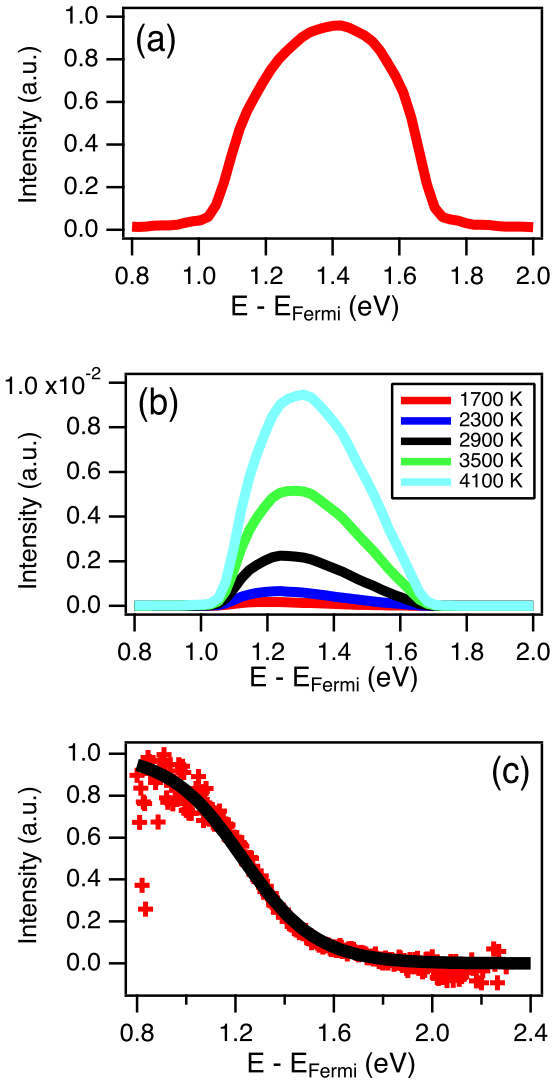

FIG. 3. (a) Theoretical density of states for the UHB calculated using DMFT. (b) Calculated equilibrium occupation function at different temperatures for this model. (c) Connection between DMFT calculations and thermalized UHB population is made by showing the 2PPE data measured at 2.5-eV pump (red crosses) divided by the fitted DOS. The solid line shows the corresponding equilibrium DMFT occupation divided by the DOS at $T = 1700$ K from (b). The points are experimental data [raw 2PPE intensity divided by the best-fit DOS function *A(E)* from Fig. 2(d)] with a hot electron temperature of 1590 K.

theoretical proposals suggest that the complex many-body quantum physics in the Hubbard model can give rise to spontaneous localization of interacting polaronic quasiparticles [47] and nonthermal entanglement entropy properties [48]. This connects correlated materials to the recent theoretical interest in many-body localized phases [49], but considers the phenomena in a way that is not controlled by disorder. It is important to advance experimental characterization of thermalization effects in real correlated materials to search for these exotic possibilities. Our observations show that intraband thermalization is extremely rapid in α-$RuCl_3$ and that the

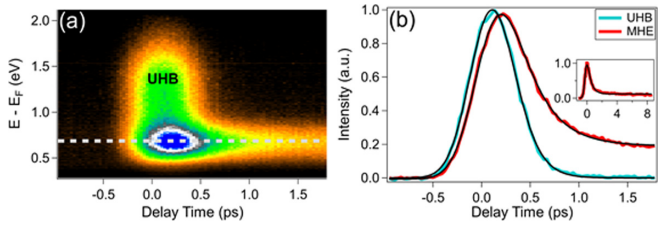

FIG. 4. (a) Photoelectron intensity map as a function of energy and pump-probe delay time for 2.5-eV pump energy; the population in the UHB region is seen to decay very rapidly. (b) Horizontal cut through the UHB and MHE regions. The UHB (cyan) shows a nearly symmetric time trace that implies a population decay of less than 200 fs The MHE (red) shows an asymmetric trace with a time constant of ∼300 fs, determined by the fit to an exponentially modified Gaussian (black). The inset shows the population of the MHE at longer delays extending the time axis of the main plot out to ∼8 ps.

creation of long-lived nonthermal populations in solids will require special conditions.

B. Time-resolved 2PPE of excited state population dynamics in α-$RuCl_3$

The 2PPE intensity as a function of pump-probe delay time for 2.5-eV pump energy is shown in Fig. 4(a). The region at about 1.0–1.5 eV above the Fermi level is associated with the UHB as described in the previous section. Intensity in this energy range only exists for a very short time indicating rapid relaxation of the doublon population. Temporal line traces show this ultrafast dynamics in Fig. 4(b), which includes a cut through the peak of the UHB at ∼1.5 eV. This time trace has only a very small asymmetry. Thus, precise quantification the UHB population decay time constant is not possible by fitting an exponentially modified Gaussian, as is often the approach in 2PPE experiments. However, based on the peak width, we can say that the decay of the doublon population in the UHB occurs significantly faster than 200 fs, which is approximately the half-width of the pump-probe temporal cross correlation.

This ultrafast timescale for doublon population decay in the UHB is initially unexpected for such a large-gap Mott insulator. Previous 2PPE studies of the smaller-gap 1T-TaS_2 showed ultrafast doublon decay of less than 20 fs, but this timescale could be rationalized based on the small gap and the involvement of defects [50]. In contrast, the energy scale set by the large gap in $RuCl_3$ should lead to significant bottlenecks in decay since low-energy elementary excitations like phonons or magnons cannot efficiently relax populations at these scales. This consideration is essentially identical to the analysis leading to the prediction [21,22] of very long doublon lifetimes in the Hubbard model that was ultimately confirmed in cold atom experiments [51].

One way to evade the bottleneck established by the large Mott gap in α-$RuCl_3$ is to consider the existence of lower-energy states within the Mott gap. The most obvious lower-energy excitation in α-$RuCl_3$ is the previously assigned excitonic band at ∼1.1-eV excitation energy [4]. We consider a very likely explanation for the observed rapid population decay in the UHB to be formation of MHEs by direct Coulomb interactions between the initially excited doublons and holons. Indeed, we see that for times after 200 fs when the intensity in the UHB energy range has disappeared, there is still photoelectron intensity at lower energies in a broad secondary distribution. However, we cannot resolve the sequential transfer of energy that would be identifiable as a temporal offset between the two time traces. The temporal offset that we observe in Fig. 4(b) can be attributed to finite resolution effects [52].

In principle, it possible to directly resolve excitonic bands in semiconductors with 2PPE, such as recently reported for Cu_2O where the excitons form very close in energy to the conduction-band edge [53]. In addition, the formation of excitons from an initial transient population of free charges has been reported for organic semiconductors via 2PPE measurements [54] and ultrafast exciton ionization in GaAs has been quantified with extraordinary time resolution [55]. In $RuCl_3$, we cannot directly resolve the exciton band as a distinct spectral feature in our 2PPE measurements due to the high work function and large exciton binding energy. However, we can indirectly assess the dynamics of the excitonic states via their influence on the hot secondary distribution. This distribution should include some population from the high-energy tail of the excitonic (called the α peak) observed in optical spectra [4]. We use the dynamical data shown in Fig. 4(a) to address the dynamics of the lower-energy hot electron populations that arise via photoemission from the excitonic states.

Figure 4(b) and its inset show time traces at lower energy of ∼0.7 eV above the Fermi level, which is well below the UHB spectral feature so that the only states available to excited electrons are in the excitonic band. In this energy range, fitting the 2PPE time trace to an exponentially modified Gaussian gives two different time constants. A statistical analysis of 45 different samples yields an average fast time constant of 370 ± 90 fs, where the error bars represent the standard deviation of 45 separate time scans similar to that in Fig. 4(b) measured on different sample positions. The order of magnitude of this timescale is consistent with relaxation via Coulomb interaction and/or energy exchange with lattice phonons [33]. We assign this relaxation as the "cooling" of excitons in the high-energy part of the excitonic band, which is a well-known process particularly for excitation energies well above the gap [56]. Since these quasiparticles are created by hot carriers in the UHB and the LHB, it is reasonable to assert that some relaxation will occur on very short timescales after they are initially created.

A much longer timescale is also evident in Fig. 4(b) and its inset that is longer than the laser repetition rate in our experiments (corresponding to 4 μs and leading to a weak signal at negative time delays; see Supplemental Material, Fig. S2 [29]). We have also extended the pump-probe delay out to ∼500 ps and not found any significant decay of the population offset indicated in Fig. 4(b). This shows the presence of a very long-lived exciton population. While we cannot quantify the precise population lifetime from these measurements, the negative time-delay signal in Fig. S2 shows that it is very long and that some excitations persist for ∼4 μs. Very similar long-lived excitations were proposed to explain 2PPE measurements of the large-gap Mott insulator UO_2 [57]. For this

material, there are also two timescales: a fast scale governing intraband carrier cooling within the UHB and a slow scale governing relaxation of exciton-polarons (suggested to be via complex phonon emission processes [57]). The difference compared to our experiments is that we find a UHB population that thermalizes and decays in less than 200 fs. After this transient, when MHEs have formed from the charged initial excitations, the similarities between UO_2 and $RuCl_3$ are striking. Evidently, the phenomenology of long-lived excitons in large-gap Mott insulators is generic. In the case of UO_2, the long lifetime was in part attributed to coupling between excitons and phonons, leading to Mott-Hubbard exciton-polarons [57]. We do not have direct evidence for polaronic effects in our experiments but it is possible that they are also relevant to $RuCl_3$. Interestingly, exciton-polarons have been recently implicated in 2D lead-halide perovskite materials via sensitive temperature-dependent spectroscopy studies [58]. The 2D nature of these materials as well the presence of halide anions further suggests that polaronic effects are important to consider in the similarly quasi-2D$RuCl_3$.

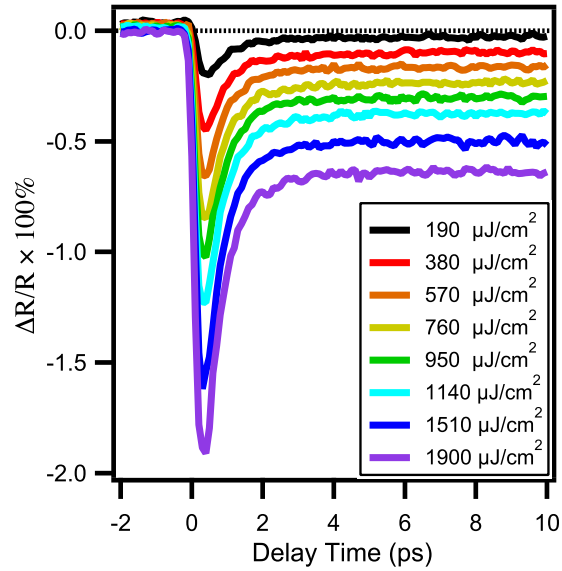

FIG. 5. Differential reflectivity at 1.15 eV due to 3.1-eV pump excitation at different pump fluences.

C. Transient reflection spectroscopy of the excitonic band in α-$RuCl_3$

In our 2PPE experiments, it is not possible to directly resolve the excitonic band in α-$RuCl_3$. Instead, we rely on the indirect observation of dynamics within the hot secondary electron background to infer the presence of photoexcitations below the threshold set by the Mott gap at ∼2-eV excitation energy. This population is evident in Fig. 2(a) in the 1.9-eV pump spectra where, despite the lack of a distinct feature at the UHB energies, there is still a smooth distribution of photoelectrons at lower energies. This necessitates the presence of photoexcited states with energies below the Mott gap energy of ∼2 eV separating the LHB and the UHB. It is indirect photoemission-based evidence for the excitonic band that is known to exist starting at 1.1-eV photon energy [4].

To make a more direct connection between the timescales in our 2PPE study and the exciton band, we now consider transient reflection spectroscopy. In these experiments, we probe with 1.15-eV photon excitation energy, corresponding to the energy associated with direct optical transition into the excitonic state that could not be directly resolved in 2PPE. Figure 5 shows the change in sample reflectance due to a 3.1-eV pump pulse as a function of delay time between the pump and the 1.15-eV probe. The differential reflection measurements permit us to directly probe the effect of the pump on the region near the excitonic peak.

In the experiment shown in Fig. 5, there is a rapid pump-induced reduction of reflectivity of the sample at 1.15-eV energy that recovers at a rate with two time constants similar to the 2PPE dynamics in Fig. 4(c). We directly confirmed the linearity of the intensity of the transient reflection dip and long-time saturation value with pump power. The fast time constant for recovery of reflectivity is ∼600 fs. This is somewhat longer than the fast timescale attributed to exciton cooling in our 2PPE measurements. Such a trend is consistent with the idea that the cooling rate is larger for excitons with energies high in the band and lower near the bottom. Furthermore, the independence of the decay rate on the pump fluence, as shown in Fig. 5, is more evidence that phonon scattering may play a significant role in the decay of this excited state as was previously discussed.

The slow time constant is once again too long to accurately measure with the ultrafast spectroscopy experiments we have carried out. Note that the reflectivity of the sample never fully recovers on the 10-ps time range in Fig. 5. The essential point is that the reflectivity changes due to photoexcitation persist for very long times. This experiment directly connects the timescales from photoemission measurements with the excitonic bands by allowing access to the lower-energy response. On this basis, we assign the long-lived excitations in this system to Mott-Hubbard excitons.

The significance of the observation of long-lived excitons comes from several contexts. First, several theoretical predictions exist [13,24] that excitons in Mott insulators should be long lived and our experiments provide more evidence that this is generic behavior. A particularly important question is when should we expect to be able to create a metal by photodoping? Though the simplest view of Mott insulators suggests that any doping should frequently lead to a metallic state [59], the existence of strongly bound excitons interfere with this expectation. In particular for large-U Mott insulators, the so-called exciton Mott-Hubbard insulator has been identified as an alternative to a metallic state when strong electron-hole interactions exist [60]. Our work on $RuCl_3$ and the related phenomenology of UO_2 [57] (the Coulomb interaction strength of 4.6 eV [57] in UO_2 is similar to the value of 4.35 eV [23] in α-$RuCl_3$), suggests that an exciton Mott insulator state could be a common outcome upon photodoping rather than a metallic state for some large-gap correlated materials. By contrast, smaller-gap Mott insulators may be more likely to achieve the photodoped metallic behavior such as has been reported for 1D organic molecular solids [61], 1T-TaS_2 [62], and VO_2 [63].

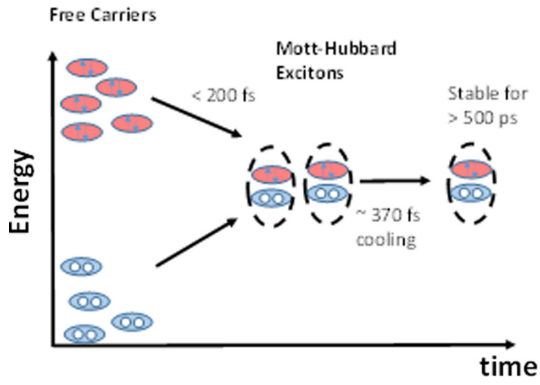

FIG. 6. Schematic illustration of the energy scales and relaxation timescales of the important photoexcitations revealed in our experiments. The pink ovals represent doublons which are transiently created in the UHB. In addition, the blue ovals show the corresponding holes created in the LHB (not directly observed in our experiments). The free carriers rapidly evolve to MHEs through Coulomb binding of doublons to holons. After a brief population relaxation by energy transfer to other degrees of freedom (exciton cooling) the MHEs persist for very long times (>500 ps).

IV. SUMMARY AND CONCLUSIONS

In summary, we have carried out time-resolved studies of several aspects of photoexcitation dynamics in the spin-orbit assisted Mott insulator α-$RuCl_3$. We observe a transient population of doublons in the upper Hubbard band that has internally thermalized on timescales too rapid to quantify in our experiments. This population decays in less than 200 fs into a lower-energy population assigned as Mott-Hubbard excitons. After a fast relaxation where the MHEs cool by exchanging energy with phonons and remnant free carriers, the MHE population is stable for very long times of up to at least 500 ps. Complementary transient reflection measurements confirm directly that these timescales are associated with the excitonic band in α-$RuCl_3$ at ∼1.1-eV excitation energy. The long lifetime of the MHEs is consistent with several recent theoretical predictions for exciton dynamics in Mott insulators [13,24]. The sequence of events controlling photoexcitation dynamics proposed from our study is illustrated schematically in Fig. 6. Not shown in this schematic is the possible stabilizing influence of low-energy species such as phonons or magnons that might contribute to the ultimate value of the MHE lifetime.

The existence of very long-lived photoexcitations in this correlated solid is significant in the search for nonequilibrium phases in quantum materials. First, the many-body channel of MHE formation and relaxation precludes realizing the prediction of long-lived doublons in this Mott insulator. We expect similar complexities to be present in other materials, noting especially the similarity to UO_2 [57]. This channel would have to be suppressed, for example, if one wanted to enhance pairing interactions in photoexcited materials for superconducting applications [64]. However, our observations suggest that we shift attention from the possibility of long-lived doublons to long-lived Mott-Hubbard excitons. This could be an interesting context to consider nonequilibrium materials phases such as electron-hole liquids [65] where transient control of excitation density can create new phases with unique optical and electronic properties. It will be exciting to see what new properties can be realized in photoexcited materials with strong electronic correlations.

ACKNOWLEDGMENTS

Surface characterization (ARPES, 2PPE, and LEED) was funded by the US Department of Energy, Office of Science, Basic Energy Sciences under Award No. DE-SC0010324. 2PPE instrumentation was funded by a UNC-GA ROI award. Theoretical modeling by A.K. and A.F.K. was supported by the National Science Foundation under Grant No. DMR-1752713. D.N. was partially funded by US Department of Energy, Office of Science, Office of Basic Energy Sciences, under Contract No. DE-SC0012704 during final manuscript preparation.

[1] A. Banerjee, J. Q. Yan, J. Knolle, C. A. Bridges, M. B. Stone, M. D. Lumsden, D. G. Mandrus, D. A. Tennant, R. Moessner, and S. E. Nagler, Science **356**, 1055 (2017).
[2] H. S. Kim, V. V. Shankar, A. Catuneanu, and H. Y. Kee, Phys. Rev. B **91** 241110(R) (2015).
[3] Y. Kubota, H. Tanaka, T. Ono, Y. Narumi, and K. Kindo, Phys. Rev. B **91**, 094422 (2015).
[4] L. J. Sandilands, C. H. Sohn, H. J. Park, S. Y. Kim, K. W. Kim, J. A. Sears, Y. J. Kim, and T. W. Noh, Phys. Rev. B **94**, 195156 (2016).
[5] F. H. L. Essler, F. Gebhard, and E. Jeckelmann, Phys. Rev. B **64**, 125119 (2001).
[6] H. Aoki, N. Tsuji, M. Eckstein, M. Kollar, T. Oka, and P. Werner, Rev. Mod. Phys. **86**, 779 (2014).
[7] M. Buzzi, M. Forst, R. Mankowsky, and A. Cavalleri, Nat. Rev. Mater. **3**, 299 (2018).
[8] T. Oka and S. Kitamura, Annu. Rev. Condens. Matter Phys. **10**, 387 (2019).
[9] H. Kishida, H. Matsuzaki, H. Okamoto, T. Manabe, M. Yamashita, Y. Taguchi, and Y. Tokura, Nature (London) **405**, 929 (2000).
[10] M. Ono, K. Miura, A. Maeda, H. Matsuzaki, H. Kishida, Y. Taguchi, Y. Tokura, M. Yamashita, and H. Okamoto, Phys. Rev. B **70**, 085101 (2004).
[11] K. W. Plumb, J. P. Clancy, L. J. Sandilands, V. V. Shankar, Y. F. Hu, K. S. Burch, H. Y. Kee, and Y. J. Kim, Phys. Rev. B **90**, 041112(R) (2014).
[12] H. Itoh, A. Takahashi, and M. Aihara, Phys. Rev. B **73**, 075110 (2006).
[13] K. A. Al-Hassanieh, F. A. Reboredo, A. E. Feiguin, I. Gonzalez, and E. Dagotto, Phys. Rev. Lett. **100**, 166403 (2008).
[14] A. Gossling, R. Schmitz, H. Roth, M. W. Haverkort, T. Lorenz, J. A. Mydosh, E. Muller-Hartmann, and M. Gruninger, Phys. Rev. B **78**, 075122 (2008).
[15] K. W. Kim, G. D. Gu, C. C. Homes, and T. W. Noh, Phys. Rev. Lett. **101**, 177404 (2008).

[16] Y. L. Li, R. D. Schaller, M. Z. Zhu, D. A. Walko, J. Kim, X. L. Ke, L. D. Miao, and Z. Q. Mao, Sci. Rep. **6**, 19302 (2016).

[17] J. Kim, D. Casa, M. H. Upton, T. Gog, Y. J. Kim, J. F. Mitchell, M. van Veenendaal, M. Daghofer, J. van den Brink, G. Khaliullin, and B. J. Kim, Phys. Rev. Lett. **108**, 177003 (2012).

[18] J. Kim, M. Daghofer, A. H. Said, T. Gog, J. van den Brink, G. Khaliullin, and B. J. Kim, Nat. Commun. **5**, 4453 (2014).

[19] Z. Alpichshev, E. J. Sie, F. Mahmood, G. Cao, and N. Gedik, Phys. Rev. B **96**, 235141 (2017).

[20] D. J. Lovinger, M. Brahlek, P. Kissin, D. M. Kennes, A. J. Millis, R. Engel-Herbert, and R. D. Averitt, Phys. Rev. B **102**, 115143 (2020).

[21] M. Eckstein and P. Werner, Phys. Rev. B **84**, 035122 (2011).

[22] N. Strohmaier, D. Greif, R. Jordens, L. Tarruell, H. Moritz, T. Esslinger, R. Sensarma, D. Pekker, E. Altman, and E. Demler, Phys. Rev. Lett. **104**, 080401 (2010).

[23] S. Sinn, C. H. Kim, B. H. Kim, K. D. Lee, C. J. Won, J. S. Oh, M. Han, Y. J. Chang, N. Hur, H. Sato, B. G. Park, C. Kim, H. D. Kim, and T. W. Noh, Sci. Rep. **6**, 39544 (2016).

[24] N. Bittner, D. Golez, M. Eckstein, and P. Werner, Phys. Rev. B **101**, 085127 (2020).

[25] H. Matsueda, S. Sota, T. Tohyama, and S. Maekawa, J. Phys. Soc. Jpn. **81**, 013701 (2011).

[26] S.-Y. Park, S.-H. Do, K.-Y. Choi, D. Jang, T.-H. Jang, J. Schefer, C.-M. Wu, J. S. Gardner, J. M. S. Park, J.-H. Park, and S. Ji, arXiv:1609.05690 (2016).

[27] J. Graf, S. Hellmann, C. Jozwiak, C. L. Smallwood, Z. Hussain, R. A. Kaindl, L. Kipp, K. Rossnagel, and A. Lanzara, J. Appl. Phys. **107**, 014912 (2010).

[28] S. Passlack, S. Mathias, O. Andreyev, D. Mittnacht, M. Aeschlimann, and M. Bauer, J. Appl. Phys. **100**, 024912 (2006).

[29] See Supplemental Material at http://link.aps.org/supplemental/10.1103/PhysRevB.103.245105 for additional experimental controls.

[30] X. Q. Zhou, H. X. Li, J. A. Waugh, S. Parham, H. S. Kim, J. A. Sears, A. Gomes, H. Y. Kee, Y. J. Kim, and D. S. Dessau, Phys. Rev. B **94**, 161106(R) (2016).

[31] S. Tougaard and B. Jorgensen, Surf. Interface Anal. **7**, 17 (1985).

[32] L. P. Oloff, M. Oura, K. Rossnagel, A. Chainani, M. Matsunami, R. Eguchi, T. Kiss, Y. Nakatani, T. Yamaguchi, J. Miyawaki, M. Taguchi, K. Yamagami, T. Togashi, T. Katayama, K. Ogawa, M. Yabashi, and T. Ishikawa, New J. Phys. **16**, 123045 (2014).

[33] U. Bovensiepen and P. S. Kirchmann, Laser Photonics Rev. **6**, 589 (2012).

[34] H. E. Elsayed-Ali, T. B. Norris, M. A. Pessot, and G. A. Mourou, Phys. Rev. Lett. **58**, 1212 (1987).

[35] M. Lisowski, P. A. Loukakos, U. Bovensiepen, J. Stahler, C. Gahl, and M. Wolf, Appl. Phys. A: Mater. Sci. Process. **78**, 165 (2004).

[36] T. Elsaesser, J. Shah, L. Rota, and P. Lugli, Phys. Rev. Lett. **66**, 1757 (1991).

[37] A. Othonos, J. Appl. Phys. **83**, 1789 (1998).

[38] P. B. Allen, Phys. Rev. Lett. **59**, 1460 (1987).

[39] J. K. Freericks, H. R. Krishnamurthy, and T. Pruschke, Phys. Rev. Lett. **102**, 136401 (2009).

[40] Y. H. Wang, D. Hsieh, E. J. Sie, H. Steinberg, D. R. Gardner, Y. S. Lee, P. Jarillo-Herrero, and N. Gedik, Phys. Rev. Lett. **109**, 127401 (2012).

[41] Y. Zhang, X. Shi, W. You, Z. Tao, Y. Zhong, F. Cheenicode Kabeer, P. Maldonado, P. M. Oppeneer, M. Bauer, K. Rossnagel, H. Kapteyn, and M. Murnane, Proc. Natl. Acad. Sci. **117**, 8788 (2020).

[42] N. Tsuji and P. Werner, Phys. Rev. B **88**, 165115 (2013).

[43] M. Wais, M. Eckstein, R. Fischer, P. Werner, M. Battiato, and K. Held, Phys. Rev. B **98**, 134312 (2018).

[44] S. Reschke, F. Mayr, Z. Wang, S. H. Do, K. Y. Choi, and A. Loidl, Phys. Rev. B **96**, 165120 (2017).

[45] P. Werner and M. Eckstein, Struct. Dyn. **3**, 023603 (2016).

[46] H. Esmaielpour, V. R. Whiteside, H. P. Piyathilaka, S. Vijeyaragunathan, B. Wang, E. Adcock-Smith, K. P. Roberts, T. D. Mishima, M. B. Santos, A. D. Bristow, and I. R. Sellers, Sci. Rep. **8**, 12473 (2018).

[47] R. Q. He and Z. Y. Weng, Sci. Rep. **6**, 35208 (2016).

[48] J. R. Garrison, R. V. Mishmash, and M. P. A. Fisher, Phys. Rev. B **95**, 054204 (2017).

[49] R. Nandkishore and D. A. Huse, Annu. Rev. Condens. Matter Phys. **6**, 15 (2015).

[50] M. Ligges, I. Avigo, D. Golez, H. U. R. Strand, Y. Beyazit, K. Hanff, F. Diekmann, L. Stojchevska, M. Kallane, P. Zhou, K. Rossnagel, M. Eckstein, P. Werner, and U. Bovensiepen, Phys. Rev. Lett. **120**, 166401 (2018).

[51] R. Sensarma, D. Pekker, E. Altman, E. Demler, N. Strohmaier, D. Greif, R. Jordens, L. Tarruell, H. Moritz, and T. Esslinger, Phys. Rev. B **82**, 224302 (2010).

[52] T. Hertel, E. Knoesel, M. Wolf, and G. Ertl, Phys. Rev. Lett. **76**, 535 (1996).

[53] H. Tanimura, K. Tanimura, and P. H. M. van Loosdrecht, Phys. Rev. B **100**, 115204 (2019).

[54] E. Varene, L. Bogner, C. Bronner, and P. Tegeder, Phys. Rev. Lett. **109**, 207601 (2012).

[55] H. Tanimura and K. Tanimura, Phys. Rev. B **102**, 045204 (2020).

[56] M. Kumar, S. Vezzoli, Z. Wang, V. Chaudhary, R. V. Ramanujan, G. G. Gurzadyan, B. F. Annalisa, and C. Soci, PCCP **18**, 31107 (2016).

[57] S. M. Gilbertson, T. Durakiewicz, G. L. Dakovski, Y. W. Li, J. X. Zhu, S. D. Conradson, S. A. Trugman, and G. Rodriguez, Phys. Rev. Lett. **112**, 087402 (2014).

[58] S. Neutzner, F. Thouin, D. Cortecchia, A. Petrozza, C. Silva, and A. R. S. Kandada, Phys. Rev. Mater. **2**, 064605 (2018).

[59] M. Eckstein and P. Werner, Phys. Rev. Lett. **110**, 126401 (2013).

[60] Y. Tomio and T. Ogawa, J. Phys. Soc. Jpn. **79**, 104707 (2010).

[61] H. Okamoto, H. Matsuzaki, T. Wakabayashi, Y. Takahashi, and T. Hasegawa, Phys. Rev. Lett. **98**, 037401 (2007).

[62] L. Perfetti, P. A. Loukakos, M. Lisowski, U. Bovensiepen, M. Wolf, H. Berger, S. Biermann, and A. Georges, New J. Phys. **10**, 053019 (2008).

[63] V. R. Morrison, R. P. Chatelain, K. L. Tiwari, A. Hendaoui, A. Bruhács, M. Chaker, and B. J. Siwick, Science **346**, 445 (2014).

[64] F. Peronaci, O. Parcollet, and M. Schiro, Phys. Rev. B **101**, 161101 (2020).

[65] Y. L. Yu, A. W. Bataller, R. Younts, Y. F. Yu, G. Q. Li, A. A. Puretzky, D. B. Geohegan, K. Gundogdu, and L. Y. Cao, ACS Nano **13**, 10351 (2019).